HHS Public Access

Author manuscript

Cell Rep. Author manuscript; available in PMC 2023 February 21.

Published in final edited form as:

Cell Rep. 2023 January 31; 42(1): 111987. doi:10.1016/j.celrep.2022.111987.

GOT1 regulates CD8+ effector and memory T cell generation

Wei Xu[1,2], **Chirag H. Patel**[1,4], **Liang Zhao**[1], **Im-Hong Sun**[1], **Min-Hee Oh**[3], **Im-Meng Sun**[1], **Rachel S. Helms**[1], **Jiayu Wen**[1], **Jonathan D. Powell**[1,4,5,*]

[1]Bloomberg~Kimmel Institute for Cancer Immunotherapy, Sidney-Kimmel Comprehensive Cancer Research Center, Department of Oncology, Johns Hopkins University School of Medicine, Baltimore, MD 21287, USA

[2]Department of Pharmacology and Molecular Sciences, Johns Hopkins University School of Medicine, Baltimore, MD 21205, USA

[3]Department of Immunobiology, Yale University, New Haven, CT 06520, USA

[4]Calico LLC, South San Francisco, CA 94080, USA

[5]Lead contact

SUMMARY

T cell activation, proliferation, function, and differentiation are tightly linked to proper metabolic reprogramming and regulation. By using [U-^{13}C]glucose tracing, we reveal a critical role for GOT1 in promoting CD8$^+$ T cell effector differentiation and function. Mechanistically, GOT1 enhances proliferation by maintaining intracellular redox balance and serine-mediated purine nucleotide biosynthesis. Further, GOT1 promotes the glycolytic programming and cytotoxic function of cytotoxic T lymphocytes via posttranslational regulation of HIF protein, potentially by regulating the levels of α-ketoglutarate. Conversely, genetic deletion of GOT1 promotes the generation of memory CD8$^+$ T cells.

In brief

Xu et al. show that the metabolic enzyme GOT1 is upregulated in effector CD8$^+$ T cells and is essential for their proliferation under serine-free conditions, as well as supporting their effector functions.

Graphical Abstract

*Correspondence: poweljo@jhmi.edu.

AUTHOR CONTRIBUTIONS

W.X. and J.D.P. designed and oversaw the study; W.X., C.H.P., L.Z., I.H.S., M.H.O., I.M.S., and R.S.H. performed experiments and data analysis. I.H.S., C.H.P., and M.H.O. provided expertise in experimental design and data interpretation. J.W. helped with mouse genotyping and colony maintenance. W.X. and J.D.P. wrote the manuscript.

DECLARATION OF INTERESTS

J.D.P. is a cofounder and equity holder of Dracen Pharmaceuticals. C.H.P. and J.D.P. are current employees of Calico LLC.

SUPPLEMENTAL INFORMATION

Supplemental information can be found online at https://doi.org/10.1016/j.celrep.2022.111987.

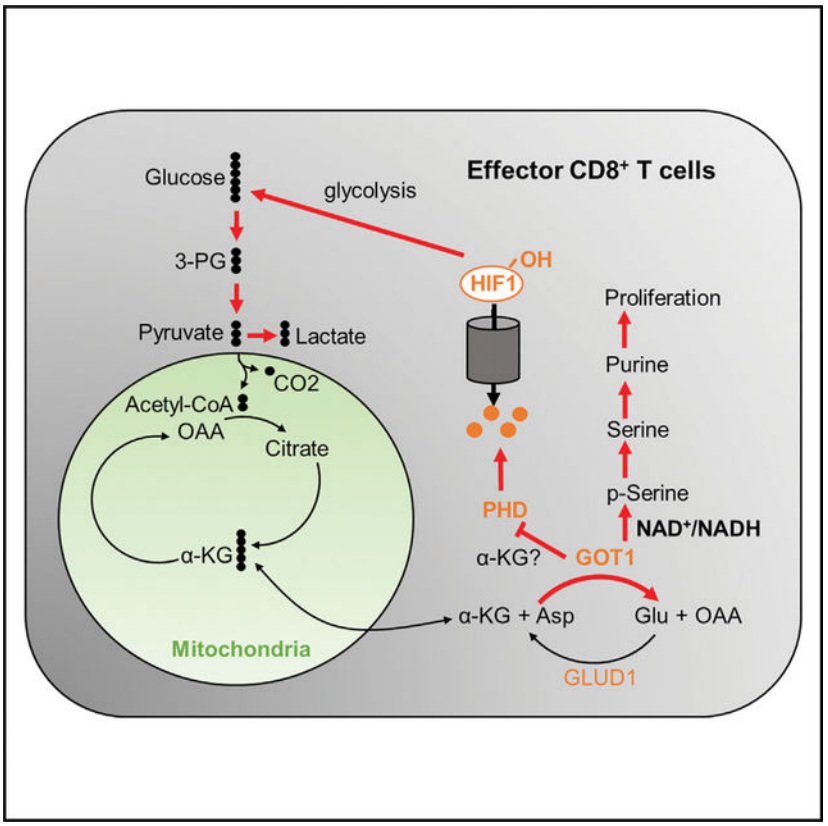

INTRODUCTION

Metabolic reprogramming plays an important role in regulating T cell activation, proliferation, function, and differentiation.[1–3] Specifically, activated T cells undergo a marked increase in glucose uptake and a subsequent upregulation of glycolysis. Rather than generating pyruvate to fuel the TCA cycle, glucose-derived pyruvate is shifted to lactate production (aerobic glycolysis).[4] In addition to aerobic glycolysis, other glucose-fueled metabolic pathways including serine biosynthesis[5–9] all contribute to T cell expansion and development.

The most abundant amino acid in serum, glutamine, and glutamine metabolism have been shown to possess important immune regulatory roles.[4,10–15] Glutaminolysis is a catabolic process where glutamine is converted to glutamate by glutaminase (GLS) and subsequently to α-ketoglutarate (α-KG) to anaplerotically feed into the TCA cycle. The role of glutaminolysis in regulating immune cell function has been studied by pharmacological inhibition or genetically deleting GLS.[16] Following GLS, glutamate can be converted to α-KG by two distinct pathways, the transaminase reaction or the glutamate dehydrogenase 1 (GLUD1) reaction. Transaminases catalyze the reversible transamination reaction between an amino acid and an α-ketoacid to generate non-essential amino acids (NEAAs). The GLUD1 reaction converts glutamate to α-KG where ammonia is generated as a by-product. How these two pathways downstream of GLS are utilized and regulated by $CD8^+$ T cells remains to be elucidated. In this report, we revealed a critical role for glutamate

oxaloacetate transaminase 1 (GOT1) in promoting effector $CD8^+$ T cell function while negatively regulating memory $CD8^+$ T cell generation.

RESULTS

Increased metabolic flux from α-ketoglutarate to glutamate upon $CD8^+$ T cell activation is mediated by increased expression of GOT1

To identify glucose-derived metabolic pathways important for $CD8^+$ T cell function, naive versus activated $CD8^+$ T cells were pulsed with [U-^{13}C]glucose. We observed a significant increase in carbon flux from glucose to glutamate, primarily indicated by M+2% and M+4% (Figure 1A). This result was unexpected as glutamine is readily converted to glutamate by GLS. We were motivated to investigate how T cells generate glutamate from glucose with ample amounts of glutamine present. Glucose-derived α-KG is converted to glutamate by GOT1 or GLUD1 (Figure 1B). To query the involvement of these two pathways, we employed aminooxyacetate (AOA) to inhibit GOT1 and epigallocatechin gallate (EGCG) to inhibit GLUD1 during $CD8^+$ T cell activation. Carbon flux from glucose to glutamate was inhibited by AOA but not EGCG (Figure 1C), indicating that GOT1, but not GLUD1, played an active role in converting glucose-derived α-KG to glutamate during $CD8^+$ T cell activation.

To specifically address this question using a genetic model, T cell conditional GOT1 or GLUD1 knockout mice (referred to as $GOT1^{-/-}$ or $GLUD1^{-/-}$ hereafter) were generated, with no overt immunologic developmental defects observed (Figures S1A–S1J). Consistent with the inhibitor results, glutamate generated from glucose was reduced in $GOT1^{-/-}$ but not $GLUD1^{-/-}$ $CD8^+$ T cells (Figures 1D and S1K, left). Of note, the absolute amount of non-glucose-derived glutamate, indicated by M+0, presumably generated from glutamine was also reduced in $GOT1^{-/-}$ cells, leading to less significant percent changes after normalizing to total glucose-derived glutamate (Figure 1D, right). Indeed, when we similarly cultured activated wild-type (WT) and $GOT1^{-/-}$ $CD8^+$ T cells using [U-^{13}C]glutamine, the absolute amount of glutamine-derived glutamate indicated by M+5 was reduced in $GOT1^{-/-}$ $CD8^+$ T cells (Figure 1E, left). Percent contribution from glutamine to glutamate indicated by M+5% was slightly increased in $GOT1^{-/-}$ $CD8^+$ T cells (Figure 1E, right), suggesting a compensatory mechanism when glucose flux to glutamate is inhibited upon GOT1 deficiency. Flux from glutamine to glutamate was not inhibited when GLUD1 was deleted (Figure S1L). Overall, these results suggest that upon $CD8^+$ T cell activation, flux from α-KG to glutamate is increased, not only from glutamine but particularly from glucose, through active GOT1 but not GLUD1.

We next sought to evaluate whether these proteins were differentially regulated during $CD8^+$ T cell activation. Upon TCR stimulation, protein expression of GOT1 was upregulated, while no significant changes in GLUD1 expression were seen (Figure 1F). As previously shown in mammary epithelial cells,[18] we hypothesized that proliferating effector and quiescent memory $CD8^+$ T cells would show preferential utilization of these two pathways. Using *In vitro* generated effector and memory $CD8^+$ T cells,[17] we observed higher GOT1 in IL-2 expanded effector $CD8^+$ T cells, but higher GLUD1 in IL-7/15 expanded memory $CD8^+$ T cells (Figure 1G). To further confirm these findings *in vivo*, effector and memory

$CD8^+$ T cells were generated using an LCMV Armstrong infection model. Consistent with our *in vitro* findings, we saw higher expression of GOT1 in effector $CD8^+$ T cells and higher GLUD1 expression in memory $CD8^+$ T cells (Figure 1H). These results suggest activated and highly proliferative effector $CD8^+$ T cells preferentially employ GOT1, rather than GLUD1, to support glutamate metabolism.

GOT1 supports serine biosynthesis and promotes $CD8^+$ T cell proliferation under serine-restricted conditions

Next, targeted metabolomics was carried out as an unbiased way to analyze metabolic changes upon GOT1 deletion in activated $CD8^+$ T cells. We observed an accumulation of aspartate concomitant with a reduction of glutamate in $GOT1^{-/-}$ $CD8^+$ T cells (Figure S2A), confirming the directionality of the GOT1 reaction (Figure 1B). Pathway enrichment analysis identified glutamate metabolism as the most significantly affected metabolic pathway (Figure S2B).

Glutamate is a critical substrate for transaminases to synthesize NEAAs (Figure S2C). The abundance of NEAAs were analyzed. 3-phospho-serine and serine were significantly reduced in $GOT1^{-/-}$ $CD8^+$ T cells (Figure 2A), suggesting an essential role for GOT1 in supporting serine biosynthesis. Serine biosynthesis is a side pathway starting from the glycolytic intermediate 3-phosphoglycerate, and serine is then generated through three serial reactions catalyzed by phosphoglycerate dehydrogenase (PHGDH), phosphoserine aminotransferase 1 (PSAT1) and phosphoserine phosphatase (PSPH) (Figure S2C). PSAT1 was highly upregulated in *in vitro* activated $CD8^+$ T cells (Figure S2D) and in *in vivo* generated effector $CD8^+$ T cells (Figure S2E), suggesting robust serine biosynthesis programming in activated effector $CD8^+$ T cells. Consistent with the reduction of total serine, carbon flux from glucose to serine indicated by M+3% was significantly reduced in $GOT1^{-/-}$ $CD8^+$ T cells (Figure 2B).

Both exogenous and *de novo* synthesized serine have been shown to be critical for $CD8^+$ T cell expansion.[5,6] We thus hypothesized that GOT1 might play a role in $CD8^+$ T cell proliferation by supporting serine biosynthesis. In complete RPMI media, which contains 0.3 mM serine, $GOT1^{-/-}$ $CD8^+$ T cells showed a minimal defect in proliferation (Figure 2C). However, in serine-free media, a significant delay in proliferation was observed with $GOT1^{-/-}$ $CD8^+$ T cells (Figure 2C). In an *in vivo* co-adoptive transfer and *Listeria monocytogenes* expressing OVA (LMOVA) infection model (Figure S2F), we observed a minimal decrease in $GOT1^{-/-}$ $CD8^+$ T cell numbers (Figure S2G, left) and proliferation (Figure S2G, right) with no significant differences in cell number at peak of infection (Figure S2H). As an NEAA, it is possible that serine generated and released from other GOT1-sufficient cells serve to overcome the defects of $GOT1^{-/-}$ T cells. Indeed, when we co-cultured WT and $GOT1^{-/-}$ $CD8^+$ T cells at 1:1 ratio (Figure S2I) in serine-free media, no significant proliferation defect of knockout cells was noted (Figure 2D).

GOT1 supports serine biosynthesis through regulation of cellular redox balance and purine nucleotide synthesis

To investigate which metabolite secreted from WT cells rescued the proliferation defect of GOT1$^{-/-}$ CD8^{+} T cells, we performed targeted metabolomics analysis of metabolites in media after activated WT CD8^{+} T cell culture. Unexpectedly, we saw a net reduction of serine after 30 h of cell culture in the media, suggesting serine might not be secreted by WT CD8^{+} T cells but rather exogenously consumed (Figure S2J). Surprisingly, pyruvate levels were most significantly enriched in the CD8^{+} T cell culture media as early as 10 h after activation (Figure 2E). As a positive control, we also observed significantly increased lactate levels in CD8^{+} T cell culture media, but much later than pyruvate (Figure S2K). The [U-^{13}C]glucose tracing experiment confirmed that pyruvate was secreted upon CD8^{+} T cell activation as a metabolite through glycolysis (Figure S2L).

Next, we tested if pyruvate supplementation could rescue the proliferation defect of GOT1$^{-/-}$ CD8^{+} T cells under serine-free conditions. 1 mM pyruvate nearly completely rescued the proliferation defect of GOT1$^{-/-}$ CD8^{+} T cells (Figure 2F). It has been reported that reduced NAD^{+}/NADH ratio constrains serine biosynthesis, leading to proliferation defects under serine-free conditions but not in serine-replete media as exogeneous serine could be used alternatively to fuel proliferation.[19] Indeed, we observed significant reduced NAD^{+}/NADH ratio in GOT1$^{-/-}$ CD8^{+} T cells (Figure 2G). These observations suggest that as an electron acceptor, pyruvate rescued the proliferation of GOT1$^{-/-}$ CD8^{+} T cells under serine-free conditions by correcting the ratio of NAD^{+}/NADH. To confirm the rescue effect of pyruvate is due to the regeneration of NAD^{+} through lactate dehydrogenase (LDH), rather than fueling the TCA cycle as an energy source, α-ketobutyrate (αKB), which has been shown to be reduced to α-hydroxybutyrate to regenerate NAD^{+},[19,20] was used as an alternate rescue reagent. Similar to pyruvate, αKB was also able to rescue the proliferation defect of GOT1$^{-/-}$ CD8^{+} T cells under serine-free conditions (Figure 2H). Collectively, our data suggested that a dysregulated NAD^{+}/NADH ratio rendered GOT1$^{-/-}$ CD8^{+} T cells sensitive to serine deprivation.

Next, WT and GOT1$^{-/-}$ CD8^{+} T cells cultured with or without serine were subjected to targeted metabolomics analysis. Principal component analysis identified four distinct clusters as WT CD8^{+} T cells with or without serine clustered closely, while GOT1$^{-/-}$ CD8^{+} T cells showed more dramatic differences with or without serine (Figure S2M). Enrichment analysis revealed purine and pyrimidine metabolic pathways to be most significantly affected upon serine addition to GOT1$^{-/-}$ CD8^{+} T cells (Figures S2N and S2O).

Consistently, purine depletion is previously reported as a major consequence of reduced intracellular serine availability, particularly when NAD^{+} regeneration was impaired.[19] We mapped out significantly affected purine and pyrimidine metabolites from our metabolomics data (Figure S2P), and reduced levels of AMP and GMP concomitant with increased purine precursor AICAR in GOT1$^{-/-}$ CD8^{+} T cells under serine-free conditions suggested a limitation of 10-formyltetrahydrofolate (10-CHO-THF), whose formation relies on one-carbon (1C) units from serine, to facilitate the conversion of AICAR. Restoring 1C units by supplementing cells with sodium formate partially rescued the proliferation of GOT1$^{-/-}$ CD8^{+} T cells under serine-free conditions (Figure 2I). Besides, salvage of purine

nucleobases by adding hypoxanthine or directly adding the purine nucleobase adenine was able to partially rescue the proliferation of GOT1$^{-/-}$ CD8^{+} T cells (Figure 2I). These results suggest GOT1 supports CD8^{+} T cell proliferation by facilitating serine and purine nucleotide biosynthesis.

GOT1 posttranslationally regulates HIF1α expression and the cytotoxic function of CTLs

The expected direct consequence of GOT1 deficiency is an accumulation of the reactants. Interestingly, even though aspartate was significantly accumulated (Figure S2A), we observed a net reduction of α-KG levels in GOT1$^{-/-}$ CD8^{+} T cells (Figure 3A), which might suggest higher activity of α-KG utilizing pathways in GOT1$^{-/-}$ CD8^{+} T cells. When we cultured WT and GOT1$^{-/-}$ CD8^{+} T cells in [U-^{13}C]glucose or [U-^{13}C]glutamine, absolute amounts of carbon from glucose or glutamine to α-KG were both reduced with no significant changes in percent contributions were seen (Figure S3A), suggesting the reduction in total α-KG amount is due to higher consumption rather than reduced glycolysis or TCA flux.

Besides as an energy fuel, α-KG is an essential substrate for other enzymes, including prolyl hydroxylases (PHDs).[22] PHDs are α-KG- and oxygen-dependent protein hydroxylases and function by hydroxylating hypoxia-inducible factor 1 (HIF1, HIF1α, and HIF1β) for proteasomal degradation. Upon GOT1 deletion, we predicted that increased consumption of α-KG may lead to increased PHD activity and low HIF1 protein expression. Indeed, we saw significantly reduced HIF1α 24 h after T cell activation in GOT1$^{-/-}$ CD8^{+} T cells (Figure 3B). HIF1α can be regulated by c-MYC or mammalian target of rapamycin complex 1 (mTORC1). To this end, we did not observe changes in c-MYC levels or mTORC1 activity indicated by p-S6K and p-S6 (Figure 3B). Moreover, mRNA levels of *Hif1α* were equivalent between WT and GOT1$^{-/-}$ CD8^{+} T cells (Figure 3C). As a product, succinate is known to inhibit PHDs. Compared with WT CD8^{+} T cells, GOT1$^{-/-}$ CD8^{+} T cells were resistant to dimethyl-succinate—a cell-permeable mimetic of succinate—induced HIF1α accumulation (Figure 3D), suggesting hyperactive PHD activity in GOT1$^{-/-}$ CD8^{+} T cells. When cells were cultured under hypoxia conditions, the difference in HIF1α protein expression between WT and GOT1$^{-/-}$ CD8^{+} T cells was mitigated due to limited PHD activity by the lack of oxygen (Figure 3E). In the absence of GOT1, increased hydroxylation of HIF1α at Pro564 site was observed after normalizing to total HIF1α protein levels (Figure 4F). Proteasomal inhibition with MG132 treatment in GOT1$^{-/-}$ CD8^{+} T cells led to a greater fold increase in HIF1α levels when compared with vehicle control. As a control, after MG132 treatment, we observed an equivalent fold increase of c-MYC, which is also posttranslationally regulated by proteasomal degradation but in a non-α-KG-dependent manner (Figures 3G and 3H). These results suggest that GOT1 stabilizes HIF1α, potentially by depleting α-KG and restricting the activity of PHDs, leading to reduced hydroxylation and proteasomal degradation of HIF1α.

HIF1 has been shown to promote glycolytic activity and perforin production and impair memory potential of cytotoxic T lymphocytes (CTLs).[21] We generated WT and GOT1$^{-/-}$ CTLs as previously described.[21] Protein levels of HIF1α were reduced in GOT1$^{-/-}$ CTLs (Figure 3I) with no observed changes in mRNA levels (Figure S3B). In GOT1$^{-/-}$ CTLs,

mRNA expression of HIF1α-dependent glucose transporter 1 (GLUT1) encoded by *Slc2a1* and hexokinase 2 (HK2) encoded by *Hk2* was reduced (Figure S3B). Accordingly, a reduction in glycolytic capacity was observed in GOT1$^{-/-}$ CTLs (Figure S3C). Consistent with HIF1β knockout CTLs,[21] GOT1$^{-/-}$ CD8^{+} CTLs showed reduced perforin production (Figure S3D). To further assess the cytotoxic function of these CTLs, we co-cultured OT-I CTLs with EL4 tumor cells expressing OVA (EL4-OVA), and again, GOT1$^{-/-}$ CTLs showed reduced perforin production (Figure 3J) and diminished tumor killing ability (Figure 3K). In an *in vivo* killing assay, we saw increased percentages of surviving target cells in GOT1$^{-/-}$ mice suggesting diminished killing capability of GOT1$^{-/-}$ CD8^{+} T cells (Figures S3E and S3F). Furthermore, in the B16-OVA adoptive cellular therapy model, GOT1$^{-/-}$ CD8^{+} OT-I cells showed diminished tumor controlling capacity compared with their WT counterparts (Figure 3L). We thus illustrate that in effector CD8^{+} T cells, GOT1 promotes the stabilization of HIF1α for proper glycolytic programming and cytotoxic function of CTLs.

To show the reduced glycolytic programming, perforin production, and killing ability of GOT1$^{-/-}$ CD8^{+} T cells was due to reduced HIF1α, we employed CRISPR editing to delete VHL (the E3 ligase responsible for proteasomal degradation of HIF1α) as a means to stabilize HIF1α (Figure 3M). HIF1α stabilization by knocking out VHL rescued the glycolytic capacity of GOT1$^{-/-}$ CD8^{+} T cells (Figure S3G). VHL knockout GOT1$^{-/-}$ CD8^{+} T cells showed increased perforin production and killing ability compared with control GOT1$^{-/-}$ CD8^{+} T cells (Figures 3N and 3O). Moreover, a PHD inhibitor DMOG was employed as an alternate way to stabilize HIF1α and was able to rescue the glycolytic programming, perforin production, and killing ability of GOT1$^{-/-}$ CD8^{+} T cells (Figures S3H–S3L). These results suggest reduced HIF1α expression leads to impaired CD8^{+} T cell effector function upon GOT1 deficiency.

Deletion of GOT1 promotes memory CD8^{+} T cell generation

Similar to HIF1β knockout CD8^{+} CTLs,[21] GOT1$^{-/-}$ CD8^{+} CTLs showed enhanced expression of central memory marker CD62L (Figure 4A). When we co-adoptively transferred WT and GOT1$^{-/-}$ CTLs into WT recipients at 1:1 ratio (Figure 4B, left), more GOT1$^{-/-}$ CD8^{+} T cells were recovered in the spleen and lymph nodes (Figure 4B, right panel). Glycolysis is shown to regulate effector and memory CD8^{+} T cell differentiation, and low glycolytic activity promotes the generation of memory CD8^{+} T cells.[23] We hypothesize that knocking out GOT1 might promote the generation of long-lived memory CD8^{+} T cells as a consequence of reduced HIF1α expression and glycolysis.

To show a cell intrinsic role of GOT1 in regulating CD8^{+} T cell memory generation, we adoptively transferred WT and GOT1$^{-/-}$ OT-I CD8^{+} T cells into WT recipients and infected the recipient mice with LMOVA (Figure 4C). No differences in the absolute number of OT-I cells at the peak of infection were noted (Figure 4D). Alternatively, we observed GOT1$^{-/-}$ CD8^{+} T cells with a decreased percentage of terminally differentiated KLRG1^{+}CD127^{-} CD8^{+} T cells and an increase in percentage of KLRG1^{-}CD127^{+} memory precursor cells (Figure 4E). When we re-challenged the T cells *ex vivo* using OVAI peptide, GOT1$^{-/-}$ OT-I cells made significantly more IL-2, which is tightly associated with central memory T cell

generation (Figure 4F). More GOT1$^{-/-}$ CD8^{+} T cells were recovered before (Figure 4G, left) and after rechallenge with VacOVA (Figure 4G, right). Moreover, GOT1$^{-/-}$ CD8^{+} cells showed a survival advantage over their WT counterparts during memory formation in a co-adoptive transfer model (Figures 4H–4J). Together, these results suggest that by deleting GOT1, CD8^{+} T cells exhibit an enhanced capacity to become long-lived memory T cells.

DISCUSSION

In this study, we showed that upon CD8^{+} T cell activation, carbon flux from α-KG (derived from glutamine and particularly from glucose) to glutamate was increased through GOT1. As glutaminolysis is defined as the catabolism of glutamine to glutamate and subsequently to α-KG, it was intriguing for us to investigate the role of GOT1, which converts α-KG back to glutamate, which seems paradoxical to the purpose of glutaminolysis, upon CD8^{+} T cell activation. Rather than a simple equilibrium between α-KG and glutamate, we now illustrate that GOT1 is essential for CD8^{+} T cell proliferation by maintaining serine biosynthesis (under serine-restricted conditions), while it also regulates HIF1 at the posttranslational level.

The reduction in total glutamate levels upon GOT1 deficiency prompted us to look into NEAAs, as glutamate is an important substrate for multiple NEAA synthesizing transaminases. We surprisingly observed significantly reduced 3-phospho-serine and serine, but not any other NEAAs, which suggested to us GOT1 might not be controlling overall NEAA synthesis through the generation of glutamate but rather contributes to serine biosynthesis via different mechanisms. In this aspect, the ultimate fate of glutamate generated through GOT1 remains to be discovered.

Even though GOT1 contributes to serine synthesis in normal media, the proliferation defect of GOT1$^{-/-}$ CD8^{+} T cells was only seen in serine-free media when T cells became solely dependent on *de novo* serine synthesis. Interestingly, the proliferation defect of GOT1$^{-/-}$ CD8^{+} T cells could be rescued by the presence of their WT counterparts under serine-restricted conditions, suggesting ongoing transfer of metabolites between neighboring T cells. To our surprise, we found that pyruvate was one of the most significantly secreted metabolites by activated CD8^{+} T cells. Early secretion of pyruvate by newly activated CD8^{+} T cells might be due to delayed upregulation of LDH, which converts pyruvate to lactate, as extracellular lactate accumulated much later than pyruvate. Serine biosynthesis is highly sensitive to intracellular redox balance as PHGDH, the first step of serine synthesis, requires NAD^{+} as a co-factor. As part of the malate-aspartate shuttle, GOT1 facilitates the transferring of NADH generated from glycolysis into mitochondria.[24] Upon GOT1 deficiency, a dysregulated NAD^{+}/NADH ratio led to impaired serine levels and ultimately purine nucleotide biosynthesis.

Here, we have shown the relevance of the GOT1-α-KG-PHDs axis in the posttranslational regulation of HIF1 protein expression. PHDs, especially PHD3, are very sensitive to the α-KG pools.[25] α-KG is a concentration-dependent, strong activator of PHDs.[26,27] We thus propose that upon GOT1 deletion, a “presumable” accumulation of α-KG would lead to increased PHD activity, and hyperactive PHDs eventually lead to a net reduction

of α-KG levels in GOT1$^{-/-}$ CD8^{+} T cells. Previous studies have reported that α-KG accumulates under hypoxic conditions and upon VHL loss in a WT setting,[28–31] suggesting blocking PHDs/HIF1 degradation would lead to increased intracellular α-KG levels, which is consistent with what we expect. However, whether this is also the case in GOT1$^{-/-}$ CD8^{+} T cells remains to be investigated.

Limitations of the study

In this study, we suggest that GOT1 regulates HIF1 protein expression by affecting α-KG levels and PHD activity. However, orthogonal experiments to show the reduced α-KG level in GOT1$^{-/-}$ CD8^{+} T cells was due to hyperactive PHDs need to be done. Moreover, alternate mechanisms as to how GOT1 regulates HIF protein expression need to be investigated. It remains unclear how GOT1 regulates memory CD8^{+} T cell differentiation.

STAR★METHODS

RESOURCE AVAILABILITY

Lead contact—Further information and requests for resources and reagents should be directed to and will be fulfilled by the lead contact, Jonathan D. Powell (poweljo@jhmi.edu).

Materials availability—This study did not generate new, unique reagents.

Data and code availability

- All data is available in the main text and supplemental figures.
- All metabolomics data has been deposited at National Metabolomics Data Repository and is publicly available as of the date of publication. The original codes are listed in the key resources table.
- Any additional information required to reanalyze the data reported in this paper is available from the lead contact upon request.

EXPERIMENTAL MODEL AND SUBJECT DETAILS

Cell lines—B16-OVA melanoma cells (gift of Hyam Levitsky) and EL4-OVA tumor cells were *in vitro* cultured under OVA selection media containing 400 μg mL^{-1} G418 (Life technologies).

Mice—Mice were kept in accordance with guidelines of the Johns Hopkins University Institutional Animal Care and Use Committee. 6–10 weeks old male or female mice were used for all experiments. Wild-type C57BL/6J, *Cd4*-Cre, CD90.1, CD45.1, OT-I TCR transgenic mice were obtained from Jackson Laboratories and bred in-house. P14 TCR transgenic mice were kindly provided by Dr. David A. Hildeman (Cincinnati Children's Medical Center). Mice with *loxP* flanked *Got1* exon 2 alleles were rederivatized from frozen sperms by MRC Harwell Institute (Mary Lyon Center, Harwell Campus, Oxfordshire, OX11 ORD, UK). Mice with *loxP* flanked *Glud1* alleles were kindly provided by Dr. Pierre Maechler (University of Geneva). T cell specific GOT1 or GLUD1 knockout mice were

generated by breeding *Got1* or *Glud1* floxed mice with *Cd4*-Cre mice. Mice were housed in a specific pathogen free animal facility on a 12 light/12 dark light cycle, 68–77F, and 30–70% humidity.

METHOD DETAILS

T cell activation and cytokine production—T cells were cultured in RPMI 1640 (Corning, Cat#: 10-040-CV) supplemented with 10% FBS (Gemini Bioproducts), 2 mM L-glutamine (Corning, Cat#: 25-005-CI), 10 mM HEPES (Corning, Cat#: 25-060-CI), 1% penicillin/streptomycin, 50 μg mL^{-1} gentamycin (Quality Biological), non-essential amino acids (100X, Gibco), and 50 μM β-mercaptoethanol (Sigma). For peptide activation, splenocytes from OT-I transgenic mice were activated with OVAI peptide (100 ng mL^{-1}) at cell concentration 5 E^6 mL^{-1}. For plate-bound anti-CD3 activation, $CD8^+$ T cells were isolated (MojoSort™ Mouse CD8 T cell Isolation Kit, Cat#: 480035, Biolegend). 2 million cells at concentration 1 E^6 mL^{-1} were activated in 6-well plate coated with 5 μg mL^{-1} anti-mouse CD3 (clone 2C11, Bio X Cell) and 2 μg mL^{-1} soluble anti-mouse CD28 (clone 37.51, Bio X Cell). To assess cell proliferation, cells were pre-labelled with Cell Proliferation Dye-eFluor450 and then activated. For co-culturing WT and $GOT1^{-/-}$ $CD8^+$ T cells, cells with different congenic markers were pre-labelled with Cell Proliferation Dye-eFluor450, then activated alone or mixed at 1:1 ratio. For cytokine production, cells were stimulated 4–6 h with phorbol myristate acetate (PMA, 50 ng mL^{-1}), Ionomycin (500 ng mL^{-1}) or peptide (100 ng mL^{-1}) in the presence of Golgi-stop (BD Biosciences) for intracellular staining.

In vitro* effector and memory $CD8^+$ T cell generation—In vitro* effector and memory $CD8^+$ T cells were generated as previous described.[17] Briefly, $CD8^+$ T cells were activated with plate-bound anti-CD3 and soluble anti-CD28 or peptide for 48 h, and then expanded in IL-2 (10 ng mL^{-1}) or IL-7 (10 ng mL^{-1}) and IL-15 (20 ng mL^{-1}) until day 6.

In vitro* CTLs—In vitro* CTLs were generated as previously described.[21] In brief, lymphocytes isolated from spleens and lymph nodes of OT-I or P14 TCR transgenic mice were activated with OVAI (SIINFEKL) or gp33-41 peptide (100 ng mL^{-1}) for 48 h. Cells were then expanded in mouse IL-2 (10 ng mL^{-1}) until day 6.

***In vitro* killing—**EL4 tumor cells expressing OVA (EL4-OVA) under G418 selection were labeled with Cell Proliferation Dye-eFluor450. CTLs were generated and live cells were enriched by density gradient separation (Ficoll, GE Healthcare). Effector:Tumor cells at ratio 6:1, 4:1, 2:1, 0.5:1, 0.25:1 were co-incubated for 6–8 h. Cells were then stained with viability dye and fixed in 1% PFA until further analysis. For assessing perforin production upon CTLs and EL4-OVA co-culture, Effector:Tumor cells at 1:1 ratio was used.

Flow cytometry—All experiments were performed on a FACSCelesta (BD Biosciences) and analyzed using FlowJo software (v.10.3).

Real-time PCR—Total RNA was extracted from cells at indicated time points using TRIzol reagent (Life Technologies). cDNA was generated with ProtoScript II RT Kit (New

England BioLabs) and real-time PCR was performed using Eagle Taq Universal Master Mix (Roche) and the Applied Biosystems StepOnePlus™ 96-well Real-Time PCR. Predesigned TaqMan® Assays were purchased from Applied Biosystems: *Hif1a* (Mm00468869_m1), *Slc2a1* (Mm00441473_m1), *Hk2* (Mm00443394_m1), *Sell* (Mm00441291_m1). *18s* ribosomal RNA (Life Technologies) was used as an endogenous control.

Metabolite extraction and measurement with LC-MS/MS—Cell pellets were spun down and washed twice with pre-warmed PBS. Metabolites were immediately extracted by adding methanol:water (80:20, v/v) extraction solution, sonicated and stored at −80°C for at least 2 h to precipitate the proteins. Supernatant after centrifugation at 14,000×g for 10 min was dried under nitrogen gas. Metabolites were then reconstituted using ACN:water (50:50, v/v) overnight at 4°C. Soluble metabolites after centrifugation at 14,000×g for 10 min were subjected to targeted metabolite analysis by liquid chromatography-tandem mass spectrometry (LC-MS/MS). For measurement of extracellular metabolome, 625 μL of media was added to 375 μL acetonitrile ACN. Sample were stored at −20°C for at least 2 h followed by centrifugation at 14,000×g to precipitate any proteins. 250 μL of the supernatant was mixed with 250 μL of water and added to a 3 kDa molecular weight cut-off filter spin column (Microcon YM-3 Centrifugal Filter, Millipore). Samples were centrifuged at 14,000×g at 4°C for 30 min. The flow-through was saved for LC-MS/MS analysis. 4 μL of sample was injected and analyzed on a 5500 QTRAP triple quadrupole mass spectrometer (AB Sciex) coupled to a Prominence ultra-fast liquid chromatography (UFLC) system (Shimadzu). The instrument was operated in selected reaction monitoring (SRM) with positive and negative ion-switching mode as described. This targeted metabolomics method allows for analysis of over two hundred metabolites from a single 25-min LC-MS acquisition with a 3 ms dwell time and these analyzed metabolites cover all major metabolic pathways. The optimized MS parameters were: ESI voltage was +5,000 V in positive ion mode and −4,500 V in negative ion mode; dwell time was 3 ms per SRM transition and the total cycle time was 1.57 s. Hydrophilic interaction chromatography (HILIC) separations were performed on a Shimadzu UFLC system using an amide column (Waters XBridge BEH Amide, 2.1 × 150 mm, 2.5 μm). The LC parameters were as follows: column temperature, 40°C; flow rate, 0.30 mL min^{-1}; Solvent A, water with 0.1% formic acid; Solvent B, acetonitrile with 0.1% formic acid; a non-linear gradient from 99% B to 45% B in 25 min with 5 min of post-run time. Peak integration for each targeted metabolite in SRM transition was processed with MultiQuant software (v2.1, AB Sciex). The preprocessed data with integrated peak areas were exported from MultiQuant and re-imported into Metaboanalyst software for further data analysis (statistical analysis, principal component analysis, generating heatmap, enrichment analysis, etc.).

[U-^{13}C]glucose or [U-^{13}C]glutamine tracing—$CD8^+$ T cells were counted and resuspended in full media containing 11 mM [U-^{13}C]glucose or 4 mM [U-^{13}C]glutamine at 2 E^6 mL^{-1}. Normal FBS was substituted with dialyzed FBS. 4–6 h post incubation, cells were spun down and washed once with pre-warmed PBS and metabolites were immediately extracted by adding methanol:water (80:20, v/v) extraction solution, sonicated and stored at −80°C for at least 2 h to precipitate the proteins. Supernatant after centrifugation at 14,000×g for 10 min was dried under nitrogen gas. Metabolites were

then reconstituted using ACN:water (50:50, v/v) overnight at 4°C. Soluble metabolites after centrifugation at 14,000×g for 10 min were subjected to analysis by liquid chromatography mass spectrometry (LC-MS). LC-MS based metabolomics profiling was performed on an Agilent LC-MS system consisting of an Agilent 1290 Infinity Binary UHPLC pump and a 6520 time-of-flight mass spectrometer. Samples were analyzed in negative-ion mode. Chromatographic separations were performed using an Agilent 1290 ultra-high performance liquid chromatography system with a well plate autosampler (Agilent, Santa Clara, CA, USA). An ion pairing method was developed using a C18 column (Agilent Zorbax Extend C18, 2.1 × 150 mm, 1.8 μm) with tributylamine as an ion-pairing agent, which enables the detection of most of the metabolites in central carbon metabolism. The LC parameters were as follows: autosampler temperature, 4°C; injection volume, 2 μL; column temperature, 40°C; and flow rate, 0.25 mL min^{-1}. The solvents and optimized gradient conditions for LC were: Solvent A, 97% water/3% methanol containing 5 mM TBA and 5.5 mM acetic acid; Solvent B, methanol containing 5 mM TBA and 5.5 mM acetic acid; A non-linear gradient from 0% B to 99% B in 22 min with 5 min of post-run time. A 6520 accurate-mass Q-TOF LC-MS system (Agilent) equipped with a dual electrospray (ESI) ion source was operated in negative-ion mode for metabolic profiling. The optimized ESI Q-TOF parameters for MS experiments were: ion polarity, negative; gas temperature, 325°C; drying gas, 10 L min^{-1}; nebulizer pressure, 45 psig; capillary voltage, 4,000 V; fragmentor, 140 V; skimmer, 65 V; mass range, 50–1100 m/z; acquisition rate, 1.5 spectra s^{-1}; instrument state, extended dynamic range (1700 m/z, 2 GHz). Spectra were internally mass calibrated in real time by continuous infusion of a reference mass solution using an isocratic pump connected to a dual sprayer feeding into an electrospray ionization source. Data were acquired with MassHunter Acquisition software. A metabolite database with retention times based on the ion-pairing method was developed using Agilent MassHunter PCDL manager software. The isotopologue peak extractions were achieved by Agilent MassHunter Profinder software.

Immunoblotting—Cell pellets were washed with PBS and flash frozen using liquid nitrogen. Samples were lysed in RIPA lysis buffer with protease and phosphatase inhibitor cocktails. Proteins were detected by ECL Plus substrate (GE Healthcare). All images were obtained and protein bands were quantified using UVP Biospectrum 500 Imaging System.

Metabolic flux analysis by seahorse—Live cells were enriched by density gradient separation (Ficoll, GE Healthcare). 150,000 cells were plated per well on poly-D lysine (50 μg mL^{-1}) coated TC-treated XF96 cell culture microplate (part number 101085-004, Agilent). Glycolytic stress test was performed with XF RPMI Medium (part number 103576-100). Glycolytic capacity was determined by maximal ECAR (detected following oligomycin treatment) subtracting basal ECAR. Experiments were performed using XF96 Extracellular Flux Analyzer (Agilent). The following were injected at the indicated time interval: D-glucose (11 mM), 2-deoxyglucose (2DG, 100 mM), oligomycin (2 μM).

***In vivo* LMOVA model—**For assessing proliferation *in vivo* in the same host 48 h post infection, differentially congenically marked $CD8^+$ TCR transgenic T cells recognizing ovalbumin (OT-I) were labeled with Cell Proliferation Dye-eFluor450, mixed at 1:1 ratio (1 E^6 cells of each population) and adoptively transferred into wild-type hosts. Recipient mice

were later infected with *Listeria monocytogenes* expressing ovalbumin antigen (LMOVA) (5×10^6 cfu/mouse, i.v.). Spleens were collected 48 h after infection. To assess a regular immune response to LMOVA infection, 2000 OT-I cells, or 1000 cells of each population in the context of co-adoptive transfer, were adoptively transferred into wild-type recipients and infected. Blood, spleens and lymph nodes were collected at indicated time points. When indicated, mice were rechallenged using Vaccinia virus expressing OVA (VacOVA, 1×10^6 pfu/mouse, i.v.).

***In vivo* LCMV model—**10,000 naive Thy1.1$^+$ WT P14 cells were adoptively transferred into WT recipients and infected with LCMV Armstrong virus (2×10^5 pfu/mouse, i.p.). 7 days and 60 days post infection, Thy1.1$^+$CD8$^+$ T cells were FACS sorted.

***In vivo* killing assay—**WT and GOT1$^{-/-}$ mice were infected with VacOVA (1×10^6 pfu/mouse, i.v.). 7 days post infection, splenocytes from WT mice were labeled with high concentration of CTV, washed and loaded with OVAI peptide (3 μg mL^{-1}) for 90 min at 37°C. Cells labeled with low concentration of CTV served as internal reference. CTV^{Hi} (loaded with peptide) and CTV^{Lo} cells were mixed at 1:1 ratio and adoptively transferred into naive (WT uninfected) or infected WT, GOT1$^{-/-}$ mice. The spleens of host mice were harvested 6–12 h later. Single cells were stained with cell viability dye and fixed with 1% paraformaldehyde (PFA) after red blood cell lysis.

B16-OVA adoptive cellular therapy model—WT mice were subcutaneously implanted with 2×10^5 B16-OVA tumor cells on the back right flank. 11 days after tumor inoculation, mice were randomized into two groups and received an adoptive transfer of 1.5×10^6 activated WT or GOT1$^{-/-}$ OT-I CTLs derived from splenocytes, which had been stimulated *in vitro* with OVAI peptide (100 ng mL^{-1}) for 48 h and expanded in IL-2 (10 ng mL^{-1}) for an additional 48 h. On day 4 post-activation, cells were subjected to Ficoll (GE Healthcare) gradient to enrich for viable CD8$^+$ T cells. Tumor burden was assessed every 2 to 4 days by measuring length and width of tumor. Tumor volume was calculated using the formula for the prolate ellipsoid, $(L \times W^2)/2$, where L represents length and is the longer of the 2 measurements and W represents width. Mice were sacrificed when tumors exceeded 2 × 2 cm or mice experienced visible signs of discomfort.

CRISPR/Cas9 RNP system—Modified single guide RNAs (sgRNAs) were designed and synthesized by Synthego. Ribonucleoproteins (RNPs) were prepared by incubating sgRNAs and Cas9 nuclease (Integrated DNA Technologies, IDT) for 10 min at room temperature. For the delivery of RNPs, isolated WT and GOT1$^{-/-}$ CD8$^+$ T cells were washed with PBS and mixed with RNPs by using P3 Primary Cell 4D-Nucleofector™ X Kit (Lonza) immediately prior to electroporation (Lonza 4D-nucleofactor™ core unit, program DN100). Electroporated cells were recovered and washed with T cell culture media. Cells were activated with plate-bound anti-CD3 and soluble anti-CD28 and expanded in IL-2. The sequences of sgRNAs are as followed:

Ctrl: 5′-GCACUACCAGAGCUAACUCA-3′;

Vhl g1: 5′- AGGUCAUCUUUGGCUCUUCA-3′;

Vhl g2: 5′- UUUGGCUCUUCAGGGAUGCG-3′;

Vhl g3: 5′- AGGGAUGCGGGGACCCAUGA-3′.

QUANTIFICATION AND STATISTICAL ANALYSIS

All graphs and statistical analysis were performed using GraphPad Prism software (v.7 and 8). A p value less than 0.05 was considered statistically significant. Error bars represent mean ± standard deviation.

Supplementary Material

Refer to Web version on PubMed Central for supplementary material.

ACKNOWLEDGMENTS

We thank Dr. Pierre Maechler at University of Geneva for kindly sharing mice with loxP flanked *Glud1* alleles. This work was supported by the National Institutes of Health (R01CA226765, R01CA229451, R01AI155602, R01AI07761, P41EB028239-01 to J.D.P.) and the Bloomberg~Kimmel Institute for Cancer Immunotherapy.

REFERENCES

1. Wang R, and Green DR (2012). Metabolic reprogramming and metabolic dependency in T cells. Immunol. Rev. 249, 14–26. 10.1111/j.1600-065X.2012.01155.x. [PubMed: 22889212]
2. Geltink RIK, Kyle RL, and Pearce EL (2018). Unraveling the complex interplay between T cell metabolism and function. Annu. Rev. Immunol. 36, 461–488. 10.1146/annurev-immunol-042617-053019. [PubMed: 29677474]
3. van der Windt GJW, and Pearce EL (2012). Metabolic switching and fuel choice during T-cell differentiation and memory development. Immunol. Rev. 249, 27–42. 10.1111/j.1600-065X.2012.01150.x. [PubMed: 22889213]
4. Wang R, Dillon CP, Shi LZ, Milasta S, Carter R, Finkelstein D, McCormick LL, Fitzgerald P, Chi H, Munger J, and Green DR (2011). The transcription factor Myc controls metabolic reprogramming upon T lymphocyte activation. Immunity 35, 871–882. 10.1016/j.immuni.2011.09.021. [PubMed: 22195744]
5. Ma EH, Bantug G, Griss T, Condotta S, Johnson RM, Samborska B, Mainolfi N, Suri V, Guak H, Balmer ML, et al. (2017). Serine is an essential metabolite for effector T cell expansion. Cell Metab. 25, 482. 10.1016/j.cmet.2017.01.014. [PubMed: 28178570]
6. Ma EH, Verway MJ, Johnson RM, Roy DG, Steadman M, Hayes S, Williams KS, Sheldon RD, Samborska B, Kosinski PA, et al. (2019). Metabolic profiling using stable isotope tracing reveals distinct patterns of glucose utilization by physiologically activated CD8(+) T cells. Immunity 51, 856–870.e5. 10.1016/j.immuni.2019.09.003. [PubMed: 31747582]
7. Berod L, Friedrich C, Nandan A, Freitag J, Hagemann S, Harmrolfs K, Sandouk A, Hesse C, Castro CN, Bähre H, et al. (2014). De novo fatty acid synthesis controls the fate between regulatory T and T helper 17 cells. Nat. Med. 20, 1327–1333. 10.1038/nm.3704. [PubMed: 25282359]
8. Swamy M, Pathak S, Grzes KM, Damerow S, Sinclair LV, van Aalten DMF, and Cantrell DA (2016). Glucose and glutamine fuel protein O-GlcNAcylation to control T cell self-renewal and malignancy. Nat. Immunol. 17, 712–720. 10.1038/ni.3439. [PubMed: 27111141]
9. Sagone AL Jr., LoBuglio AF, and Balcerzak SP (1974). Alterations in hexose monophosphate shunt during lymphoblastic transformation. Cell. Immunol. 14, 443–452. 10.1016/0008-8749(74)90195-6. [PubMed: 4157015]
10. Newsholme P (2001). Why is L-glutamine metabolism important to cells of the immune system in health, postinjury, surgery or infection? J. Nutr. 131, 2515S–2522S. 10.1093/jn/131.9.2515S. [PubMed: 11533304]

11. Marchingo JM, Sinclair LV, Howden AJ, and Cantrell DA (2020). Quantitative analysis of how Myc controls T cell proteomes and metabolic pathways during T cell activation. Elife 9, e53725. 10.7554/eLife.53725. [PubMed: 32022686]
12. Sinclair LV, Rolf J, Emslie E, Shi YB, Taylor PM, and Cantrell DA (2013). Control of amino-acid transport by antigen receptors coordinates the metabolic reprogramming essential for T cell differentiation. Nat. Immunol. 14, 500–508. 10.1038/ni.2556. [PubMed: 23525088]
13. Nabe S, Yamada T, Suzuki J, Toriyama K, Yasuoka T, Kuwahara M, Shiraishi A, Takenaka K, Yasukawa M, and Yamashita M (2018). Reinforce the antitumor activity of CD8(+) T cells via glutamine restriction. Cancer Sci. 109, 3737–3750. 10.1111/cas.13827. [PubMed: 30302856]
14. Leone RD, Zhao L, Englert JM, Sun IM, Oh MH, Sun IH, Arwood ML, Bettencourt IA, Patel CH, Wen J, et al. (2019). Glutamine blockade induces divergent metabolic programs to overcome tumor immune evasion. Science 366, 1013–1021. 10.1126/science.aav2588. [PubMed: 31699883]
15. Klysz D, Tai X, Robert PA, Craveiro M, Cretenet G, Oburoglu L, Mongellaz C, Floess S, Fritz V, Matias MI, et al. (2015). Glutamine-dependent alpha-ketoglutarate production regulates the balance between T helper 1 cell and regulatory T cell generation. Sci. Signal. 8, ra97. 10.1126/scisignal.aab2610. [PubMed: 26420908]
16. Johnson MO, Wolf MM, Madden MZ, Andrejeva G, Sugiura A, Contreras DC, Maseda D, Liberti MV, Paz K, Kishton RJ, et al. (2018). Distinct regulation of Th17 and Th1 cell differentiation by glutaminase-dependent metabolism. Cell 175, 1780–1795.e19. 10.1016/j.cell.2018.10.001. [PubMed: 30392958]
17. Pollizzi KN, Patel CH, Sun IH, Oh MH, Waickman AT, Wen J, Delgoffe GM, and Powell JD (2015). mTORC1 and mTORC2 selectively regulate CD8(+) T cell differentiation. J. Clin. Invest. 125, 2090–2108. 10.1172/JCI77746. [PubMed: 25893604]
18. Coloff JL, Murphy JP, Braun CR, Harris IS, Shelton LM, Kami K, Gygi SP, Selfors LM, and Brugge JS (2016). Differential glutamate metabolism in proliferating and quiescent mammary epithelial cells. Cell Metab. 23, 867–880. 10.1016/j.cmet.2016.03.016. [PubMed: 27133130]
19. Diehl FF, Lewis CA, Fiske BP, and Vander Heiden MG (2019). Cellular redox state constrains serine synthesis and nucleotide production to impact cell proliferation. Nat. Metab. 1, 861–867. 10.1038/s42255-019-0108-x. [PubMed: 31598584]
20. Sullivan LB, Gui DY, Hosios AM, Bush LN, Freinkman E, and Vander Heiden MG (2015). Supporting aspartate biosynthesis is an essential function of respiration in proliferating cells. Cell 162, 552–563. 10.1016/j.cell.2015.07.017. [PubMed: 26232225]
21. Finlay DK, Rosenzweig E, Sinclair LV, Feijoo-Carnero C, Hukelmann JL, Rolf J, Panteleyev AA, Okkenhaug K, and Cantrell DA (2012). PDK1 regulation of mTOR and hypoxia-inducible factor 1 integrate metabolism and migration of CD8+ T cells. J. Exp. Med. 209, 2441–2453. 10.1084/jem.20112607. [PubMed: 23183047]
22. Zdzisińska B, Żurek A, and Kandefer-Szerszeń M (2017). Alpha-ketoglutarate as a molecule with pleiotropic activity: well-known and novel possibilities of therapeutic use. Arch. Immunol. Ther. Exp. 65, 21–36. 10.1007/s00005-016-0406-x.
23. Sukumar M, Liu J, Ji Y, Subramanian M, Crompton JG, Yu Z, Roychoudhuri R, Palmer DC, Muranski P, Karoly ED, et al. (2013). Inhibiting glycolytic metabolism enhances CD8+ T cell memory and antitumor function. J. Clin. Invest. 123, 4479–4488. 10.1172/JCI69589. [PubMed: 24091329]
24. Birsoy K, Wang T, Chen WW, Freinkman E, Abu-Remaileh M, and Sabatini DM (2015). An essential role of the mitochondrial electron transport chain in cell proliferation is to enable aspartate synthesis. Cell 162, 540–551. 10.1016/j.cell.2015.07.016. [PubMed: 26232224]
25. German NJ, Yoon H, Yusuf RZ, Murphy JP, Finley LWS, Laurent G, Haas W, Satterstrom FK, Guarnerio J, Zaganjor E, et al. (2016). PHD3 loss in cancer enables metabolic reliance on fatty acid oxidation via deactivation of ACC2. Mol. Cell 63, 1006–1020. 10.1016/j.molcel.2016.08.014. [PubMed: 27635760]
26. MacKenzie ED, Selak MA, Tennant DA, Payne LJ, Crosby S, Frederiksen CM, Watson DG, and Gottlieb E (2007). Cell-permeating alpha-ketoglutarate derivatives alleviate pseudohypoxia in succinate dehydrogenase-deficient cells. Mol. Cell Biol. 27, 3282–3289. 10.1128/MCB.01927-06. [PubMed: 17325041]

27. Tennant DA, Frezza C, MacKenzie ED, Nguyen QD, Zheng L, Selak MA, Roberts DL, Dive C, Watson DG, Aboagye EO, and Gottlieb E (2009). Reactivating HIF prolyl hydroxylases under hypoxia results in metabolic catastrophe and cell death. Oncogene 28, 4009–4021. 10.1038/onc.2009.250. [PubMed: 19718054]

28. Cuperlovic-Culf M, Cormier K, Touaibia M, Reyjal J, Robichaud S, Belbraouet M, and Turcotte S (2016). (1)H NMR metabolomics analysis of renal cell carcinoma cells: effect of VHL inactivation on metabolism. Int. J. Cancer 138, 2439–2449. 10.1002/ijc.29947. [PubMed: 26620126]

29. Olenchock BA, Moslehi J, Baik AH, Davidson SM, Williams J, Gibson WJ, Chakraborty AA, Pierce KA, Miller CM, Hanse EA, et al. (2016). EGLN1 inhibition and rerouting of alpha-ketoglutarate suffice for remote ischemic protection. Cell 165, 497. 10.1016/j.cell.2016.03.037. [PubMed: 27058668]

30. Metallo CM, Gameiro PA, Bell EL, Mattaini KR, Yang J, Hiller K, Jewell CM, Johnson ZR, Irvine DJ, Guarente L, et al. (2011). Reductive glutamine metabolism by IDH1 mediates lipogenesis under hypoxia. Nature 481, 380–384. 10.1038/nature10602. [PubMed: 22101433]

31. Wise DR, Ward PS, Shay JES, Cross JR, Gruber JJ, Sachdeva UM, Platt JM, DeMatteo RG, Simon MC, and Thompson CB (2011). Hypoxia promotes isocitrate dehydrogenase-dependent carboxylation of alpha-ketoglutarate to citrate to support cell growth and viability. Proc. Natl. Acad. Sci. USA 108, 19611–19616. 10.1073/pnas.1117773108. [PubMed: 22106302]

Highlights

- Glucose contributes to glutamate generation through GOT1 upon $CD8^+$ T cell activation
- GOT1 supports $CD8^+$ T cell proliferation under serine-restricted conditions
- GOT1 posttranslationally regulates HIF expression
- Genetic deletion of GOT1 leads to enhanced memory $CD8^+$ T cell formation

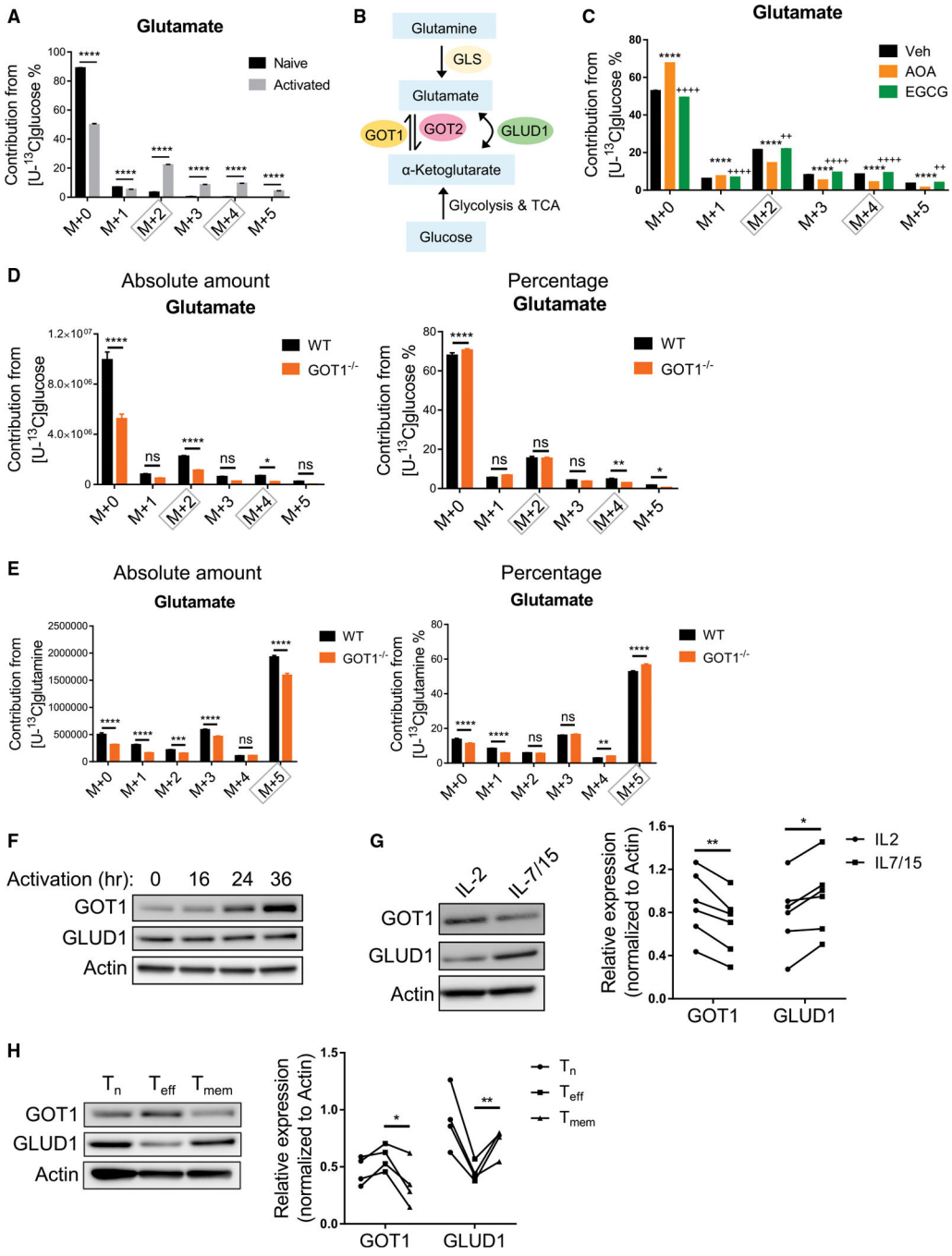

Figure 1. Increased metabolic flux from α-ketoglutarate to glutamate upon CD8$^+$ T cell activation is mediated by increased expression of GOT1

(A) Naive or 24-h plate-bound anti-CD3 and soluble anti-CD28 activated OT-I CD8$^+$ T cells were pulsed with [U-^{13}C]glucose for 4–6 h before collecting for mass spectrometry analysis. Percent contribution of carbon flux from [U-^{13}C]glucose to glutamate is shown.

(B) Graph describing the intersection of glutamine and glucose metabolism.

(C) OT-I CD8$^+$ T cells were activated with plate-bound anti-CD3 and soluble anti-CD28 in the presence of vehicle (Veh), AOA (250 μM), or EGCG (500 μM) for 24 h. Cells were then pulsed with [U-^{13}C]glucose for 4–6 h before collecting for mass spectrometry

analysis. Percent contribution of carbon flux from [U-^{13}C]glucose to glutamate is shown. *comparison between Veh and AOA, $^{+}$comparison between Veh and EGCG.

(D and E) 24-h plate-bound anti-CD3 and soluble anti-CD28 activated WT and GOT1$^{-/-}$ OT-I CD8^{+} T cells were pulsed with [U-^{13}C]glucose (D) or [U-^{13}C]glutamine (E) for 4–6 h before collecting for mass spectrometry analysis. Abundance of (left) and percent contribution (right) of carbon flux from [U-^{13}C]-glucose (D) or [U-^{13}C]glutamine (E) to glutamate are shown.

(F) Isolated OT-I or P14 CD8^{+} T cells were activated using plate-bound anti-CD3 and soluble anti-CD28. Immunoblot measurements of GOT1 and GLUD1 at indicated time points are shown. Actin served as the loading control.

(G) *In vitro* effector (IL-2) and memory (IL-7/15) OT-I or P14 CD8^{+} T cells were generated as previously described.[17] Immunoblot measurements of GOT1 and GLUD1 (left) and statistical analysis (right) are shown. Actin served as the loading control.

(H) Naive (T_n) Thy1.1^{+} P14 CD8^{+} T cells were adoptively transferred into WT recipients and infected with LCMV Armstrong. Thy1.1^{+} CD8^{+} T cells were FACS sorted on day 7 as effector T cells (T_{eff}) and on day 60 as memory T cells (T_{mem}). Immunoblot measurements of GOT1 and GLUD1 (left) and statistical analysis (right) are shown. Actin served as the loading control. *$p < 0.05$, **$p < 0.01$, ***$p < 0.001$, ****$p < 0.0001$; ns, not significant. Two-way ANOVA with Sidak's multiple comparisons test (A, C, D, and E) and paired t test (G and H). Data are representative of at least three independent experiments. Data are represented as mean ± SD. Also see Figure S1.

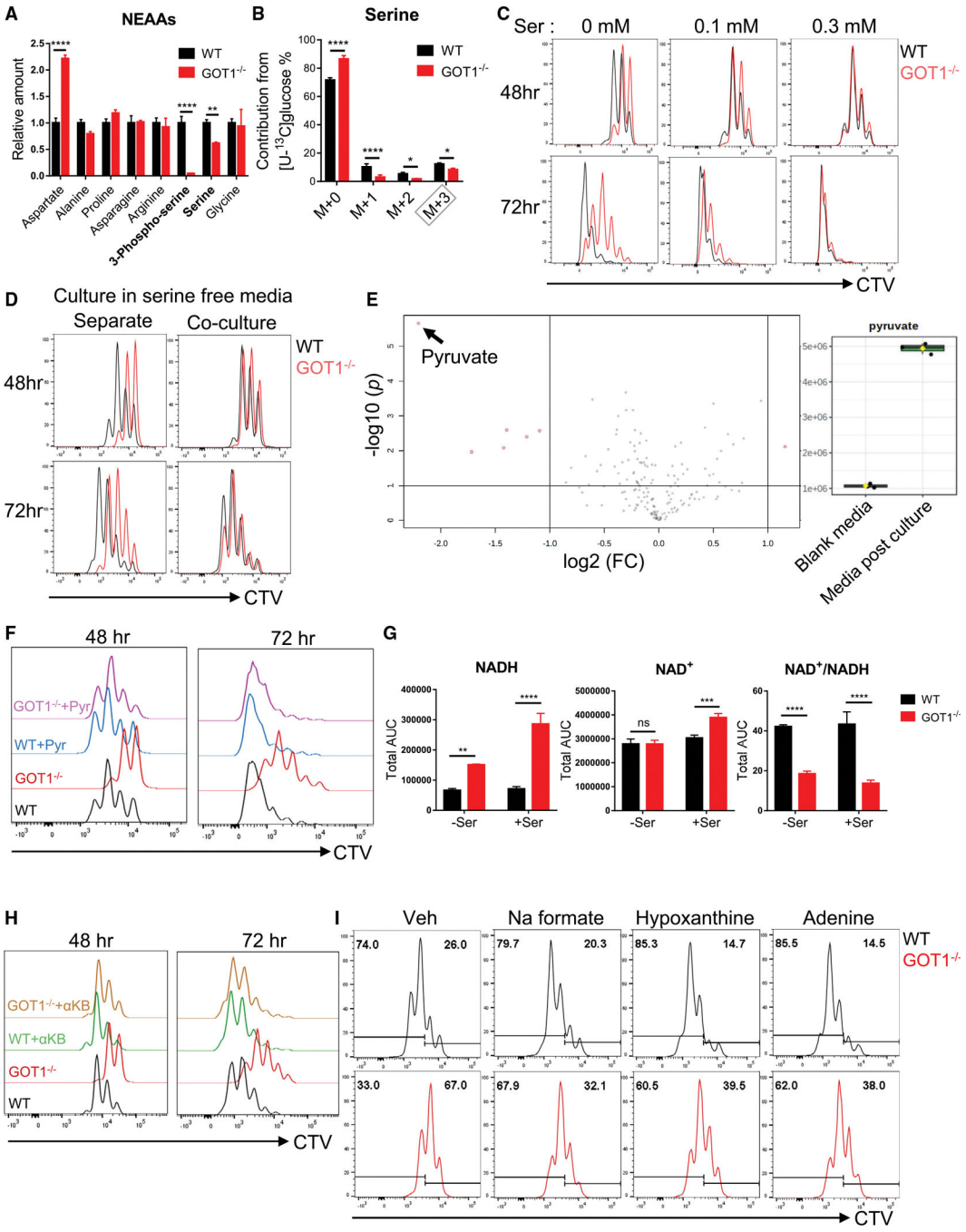

Figure 2. GOT1 supports serine biosynthesis and promotes CD8$^+$ T cell proliferation under serine-restricted conditions

(A) Abundance of non-essential amino acids (NEAAs) from targeted metabolomics analysis of 24-h activated WT and GOT1$^{-/-}$ OT-I CD8$^+$ T cells.

(B) 24-h plate-bound anti-CD3 and soluble anti-CD28 activated WT or GOT1$^{-/-}$ OT-I CD8$^+$ T cells were pulsed with [U-^{13}C]glucose for 4–6 h before collecting for mass spectrometry analysis. Percent contribution of carbon flux from [U-^{13}C]glucose to serine is shown.

(C) Flow cytometry analysis of proliferation of WT or GOT1$^{-/-}$ P14 CD8$^+$ T cells cultured under 0, 0.1, and 0.3 mM serine conditions at indicated time points.

(D) Flow cytometry analysis of proliferation of separately cultured or co-cultured WT and GOT1$^{-/-}$ P14 CD8^{+} T cells in serine-free media at indicated time points.
(E) Targeted metabolomics analysis of blank media and media after 10 h of WT OT-I CD8^{+} T cell culture. Volcano plot (left) and abundance of pyruvate (right) are shown.
(F) WT and GOT1$^{-/-}$ P14 CD8^{+} T cells were activated with plate-bound anti-CD3 and soluble anti-CD28 without or with 1 mM pyruvate (Pyr) in serine-free media. Flow cytometry analysis of proliferation at indicated time points is shown.
(G) Abundance of NADH (left) and NAD^{+} (middle) from targeted metabolomics analysis of 24-h activated WT and GOT1$^{-/-}$ OT-I CD8^{+} T cells without or with 0.3 mM serine. NAD^{+}/NADH ratios are shown (right).
(H) WT and GOT1$^{-/-}$ P14 CD8^{+} T cells were activated with plate-bound anti-CD3 and soluble anti-CD28 without or with 1 mM α-ketobutyrate (αKB) in serine-free media. Flow cytometry analysis of proliferation at indicated time points is shown.
(I) WT and GOT1$^{-/-}$ P14 CD8^{+} T cells were activated with plate-bound anti-CD3 and soluble anti-CD28 without or with 1 mM sodium formate, 200 μM hypoxanthine, or 50 μM adenine in serine-free media. Flow cytometry analysis of proliferation is shown. *$p < 0.05$, **$p < 0.01$, ***$p < 0.001$, ****$p < 0.0001$; ns, not significant. Two-way ANOVA with Sidak's multiple comparisons test (A, B, and G). Data are representative of three independent experiments. Data are represented as mean ± SD. Also see Figure S2.

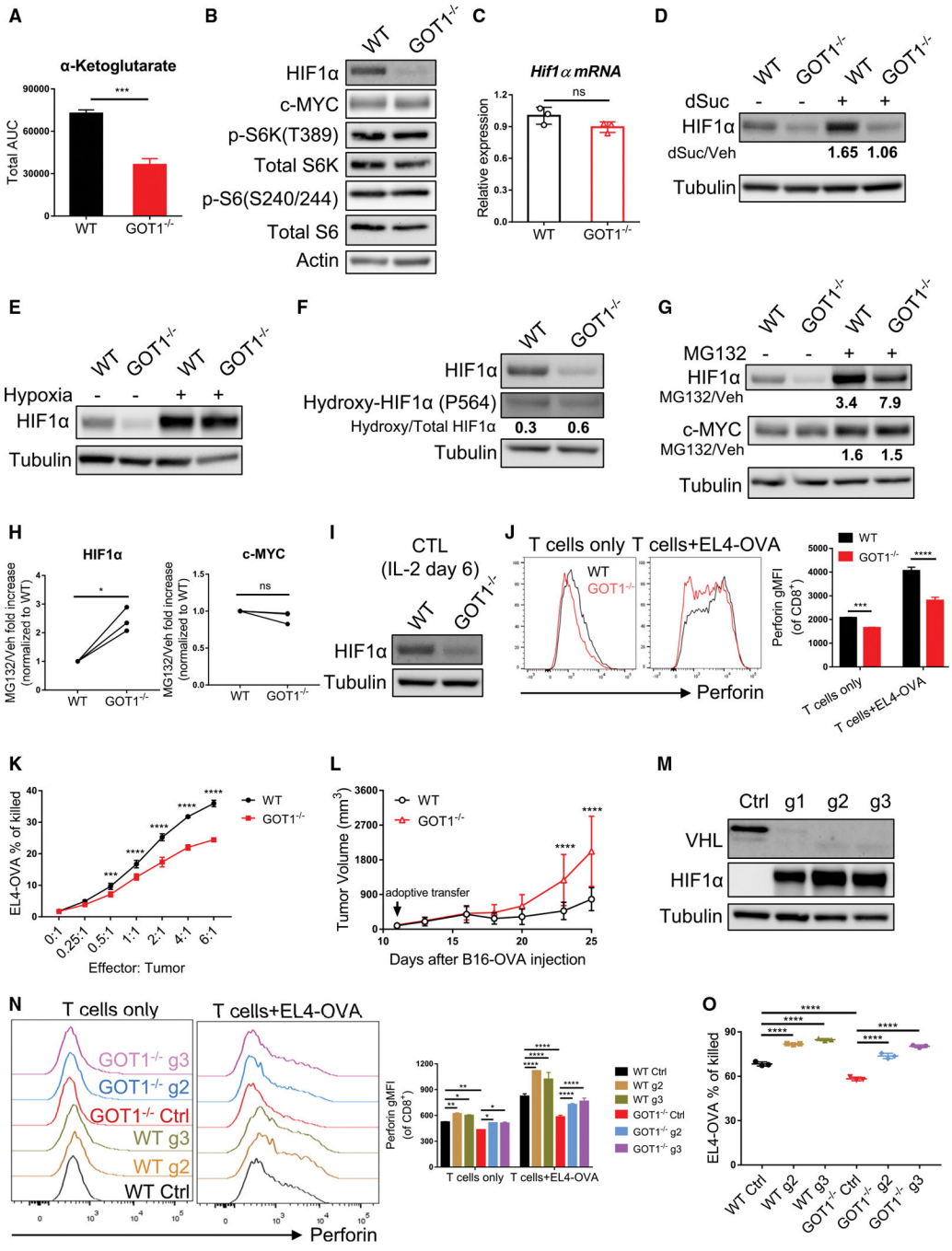

Figure 3. GOT1 posttranslationally regulates HIF1α expression and the cytotoxic function of CTLs

(A) Abundance of α-ketoglutarate from targeted metabolomics analysis of 24-h activated WT and GOT1$^{-/-}$ OT-I CD8^{+} T cells.

(B) WT and GOT1$^{-/-}$ OT-I CD8^{+} T cells were activated using plate-bound anti-CD3 and soluble anti-CD28 for 24 h. Immunoblot measurements of HIF1α, c-MYC, and mTORC1 activity indicated by p-S6K and p-S6 are shown. Total S6K, total S6, and actin served as the loading control.

(C) Real-time PCR analysis of *Hif1a* mRNA levels in 24-h plate-bound anti-CD3 and soluble anti-CD28 activated WT and GOT1$^{-/-}$ OT-I CD8^{+} T cells.
(D) WT and GOT1$^{-/-}$ OT-I CD8^{+} T cells were activated with plate-bound anti-CD3 and soluble anti-CD28 without (Veh) or with 1 mM dimethyl-succinate (dSuc) for 24 h. Immunoblot measurements of HIF1α are shown. Tubulin served as the loading control.
(E) WT and GOT1$^{-/-}$ OT-I CD8^{+} T cells were activated with plate-bound anti-CD3 and soluble anti-CD28 under normoxia for 21 h. Cells were then incubated under normoxia or hypoxia for an additional 3 h. Immunoblot measurements of HIF1α are shown. Tubulin served as the loading control.
(F) Immunoblot measurements of HIF1α and hydroxy-HIF1α at proline 564 site in 24-h activated WT and GOT1$^{-/-}$ OT-I CD8^{+} T cells. Tubulin served as the loading control.
(G and H) WT and GOT1$^{-/-}$ OT-I CD8^{+} T cells were activated with plate-bound anti-CD3 and soluble anti-CD28 for 24 h followed by 2 h of vehicle (Veh) or MG132 (10 μM) treatment. (G) Immunoblot measurements of HIF1α and c-MYC are shown. Tubulin served as the loading control. (H) Compared with vehicle control, fold increase after MG132 treatment was analyzed.
(I) OT-I or P14 CTLs were generated as previously described.[21] Immunoblot measurements of HIF1α in WT and GOT1$^{-/-}$ CTLs are shown. Tubulin served as the loading control.
(J) Flow cytometry comparison of perforin production between WT and GOT1$^{-/-}$ OT-I CTLs alone or co-cultured with EL4-OVA for 6 h. Flow plots (left panel) and statistical analysis of geometric mean fluorescence intensity (gMFI, right) are shown.
(K) Percentages of killed EL4-OVA by WT or GOT1$^{-/-}$ CTLs at indicated effector:tumor ratios.
(L) WT and GOT1$^{-/-}$ OT-I CTLs were adoptively transferred into B16-OVA tumor bearing mice on day 11 after inoculation. Measurements of tumor volume are shown.
(M) Naive WT CD8^{+} T cells were isolated and electroporated with control sgRNA (Ctrl) or sgRNAs targeting *Vhl* (g1, g2, g3) complexed with Cas9 endonuclease. Cells were recovered and activated with plate-bound anti-CD3 and soluble anti-CD28 and expanded in IL-2 until day 6. Immunoblot measurements of VHL and HIF1α are shown. Tubulin served as the loading control.
(N and O) Naive WT and GOT1$^{-/-}$ OT-I CD8^{+} T cells were isolated and electroporated with control sgRNA (Ctrl) or sgRNAs targeting *Vhl* (g2, g3) complexed with Cas9 endonuclease. Cells were activated and expanded in IL-2 until day 6, and co-incubated without or with EL4-OVA at 1:1 ratio to assess perforin production (N), or at effector:tumor 4:1 ratio to assess the percentages of tumor cells killed (O). *$p < 0.05$, **$p < 0.01$, ***$p < 0.001$, ****$p < 0.0001$; ns, not significant. Unpaired t test (A and C), paired t test (H), two-way ANOVA with Sidak's multiple comparisons test (J, K, and L), two-way ANOVA with Tukey's multiple comparisons test (N), one-way ANOVA with Tukey's multiple comparisons test (O). Data are representative of at least three independent experiments. Data are represented as mean ± SD. Also see Figure S3.

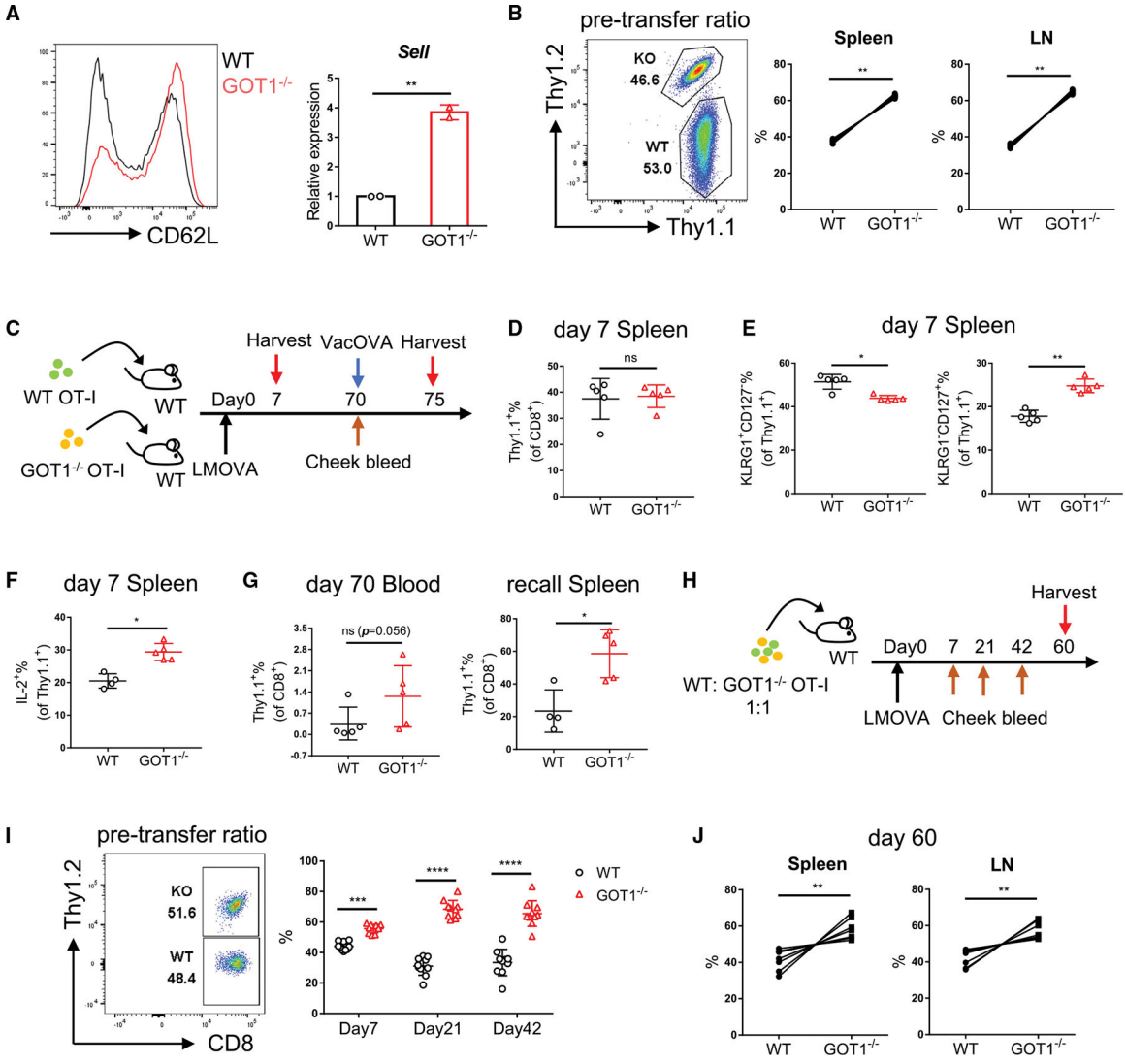

Figure 4. Deletion of GOT1 promotes memory CD8$^+$ T cell generation

(A) Flow cytometry comparison of CD62L expression (left) and real-time PCR analysis of *Sell* mRNA (right) between WT and GOT1$^{-/-}$ CTLs.

(B) WT and GOT1$^{-/-}$ CTLs with different congenic markers were mixed at 1:1 ratio and co-adoptively transferred into WT recipients. Flow cytometry analysis of percentages of WT and GOT1$^{-/-}$ CTLs before adoptive transfer (left) or from the spleen and lymph nodes 48-h after adoptive transfer (right).

(C–G) GOT1$^{-/-}$ CD8$^+$ T cells show enhanced memory generation in an adoptive transfer model. (C) Experimental scheme. Naive WT and GOT1$^{-/-}$ OT-I CD8$^+$ T cells were adoptively transferred into WT recipients separately and infected with LMOVA. (D) Percentages of antigen specific Thy1.1$^+$ cells of CD8$^+$ T cells from spleen on day 7. (E) Percentages of KLRG1$^+$CD127$^-$ and KLRG1$^-$CD127$^+$ cells of Thy1.1$^+$ T cells from spleen on day 7. (F) Percentages of IL-2$^+$ cells of Thy1.1$^+$ T cells post OVAI peptide stimulation *ex vivo* from spleen on day 7. (G) Percentages of antigen specific Thy1.1$^+$ cells

of $CD8^+$ T cells from blood on day 70 (left) and from spleen 5 days post Vaccinia-OVA (VacOVA) rechallenge (right).

(H–J) $GOT1^{-/-}$ $CD8^+$ T cells show enhanced memory generation in a co-adoptive transfer model. (H) Experimental scheme. WT and $GOT1^{-/-}$ OT-I $CD8^+$ T cells with different congenic markers were mixed at 1:1 ratio, co-transferred into WT recipients, and infected with LMOVA.

(I) Flow cytometry analysis of percentages of WT and $GOT1^{-/-}$ OT-I $CD8^+$ T cells before transfer (left) and from blood at indicated time points after adoptive transfer (right). (J) Percentages of WT and $GOT1^{-/-}$ OT-I $CD8^+$ T cells from spleen and lymph nodes on day 60. *$p < 0.05$, **$p < 0.01$, ***$p < 0.001$, ****$p < 0.0001$; ns, not significant. Unpaired t test (A), paired t test (B, J), Mann-Whitney t test (D, E, F, and G), two-way ANOVA with Sidak's multiple comparisons test (I). Data are representative of three independent experiments (A–B, D–G, and I–J). Data are represented as mean ± SD.

KEY RESOURCES TABLE

REAGENT or RESOURCE	SOURCE	IDENTIFIER
Antibodies		
GOT1	Cell Signaling Technology	Cat# 34423; RRID: AB_2799052
GLUD1	Cell Signaling Technology	Cat# 12793; RRID: AB_2750880
HIF1α	Cell Signaling Technology	Cat# 14179; RRID: AB_2622225
c-MYC	Cell Signaling Technology	Cat# 5605; RRID: AB_1903938
p-S6K	Cell Signaling Technology	Cat# 9234; RRID: AB_2269803
total S6K	Cell Signaling Technology	Cat# 9202; RRID: AB_331676
p-S6	Cell Signaling Technology	Cat# 5364; RRID: AB_10694233
total S6	Cell Signaling Technology	Cat# 2217; RRID: AB_331355
β-Tubulin	Cell Signaling Technology	Cat# 86298; RRID: AB_2715541
Hydroxy-HIF1α (Pro564)	Cell Signaling Technology	Cat# 3434; RRID: AB_2116958
β-Actin	Sigma-Aldrich	Cat# A2066; RRID: AB_476693
PSAT1	Thermo Fisher Scientific	Cat# PA5-22124; RRID: AB_11153526
Thy1.1	BD Biosciences	Cat#554898; RRID: AB_395589
Thy1.2	BD Biosciences	Cat# 553007; RRID: AB_398526
CD4	BD Biosciences	Cat# 563727; RRID: AB_2728707
IL-2	BD Biosciences	Cat# 562483; RRID: AB_11154219
CD8α	Biolegend	Cat# 100750 (RRID: AB_2562610); Cat# 100742 (RRID: AB_2563056)
CD62L	Biolegend	Cat# 104438; RRID: AB_2563058
Perforin	Biolegend	Cat# 154306 (RRID: AB_2721639); Cat# 154304 (RRID: AB_2721463)
CD127	Biolegend	Cat# 135024; RRID: AB_11218800
CD45.1	Biolegend	Cat# 110708; RRID: AB_313497
Thy1.2	Biolegend	Cat# 140319; RRID: AB_2561395
KLRG1	Thermo Fisher Scientific	Cat# 61-5893-82; RRID: AB_2574630
CD44	Thermo Fisher Scientific	Cat# 56-0441-82; RRID: AB_494011
FOXP3	Thermo Fisher Scientific	Cat# 53-5773-82; RRID: AB_763537
Fc block	Bio X Cell	Cat# 553142
Bacterial and virus strains		
LMOVA (double attenuated)	Aduro Biotech	N/A
VacOVA (double attenuated)	Aduro Biotech	N/A
LCMV Armstrong	Dr. Susan Kaech (Salk Institute)	N/A
Chemicals, peptides, and recombinant proteins		
[U-^{13}C]glucose	Cambridge Isotope Laboratories	Cat# CLM-1396
[U-^{13}C]glutamine	Cambridge Isotope Laboratories	Cat# CLM-1822

REAGENT or RESOURCE	SOURCE	IDENTIFIER
Dialyzed FBS	Invitrogen	Cat# 26400-036
RPMI 1640 without glucose	Thermo Fisher Scientific	Cat# 11879
RPMI 1640 without glutamine	Thermo Fisher Scientific	Cat# 21870
RPMI 1640 without serine and glutamine	USBiological Life Sciences	Cat# R8999-15
(Aminooxy)acetic acid hemihydrocholoride (AOA)	Sigma Aldrich	Cat# C13408
Epigallocatechin gallate (EGCG)	Sigma Aldrich	Cat# E4143
L-Serine	Sigma Aldrich	Cat# S4500
Sodium 2-oxobutyrate (αKB)	Sigma Aldrich	Cat# K0875
Sodium formate	Sigma Aldrich	Cat# 456020
Hypoxanthine	Sigma Aldrich	Cat# H9636
Adenine	Sigma Aldrich	Cat# A2786
Dimethyl-succinate (dSuc)	Sigma Aldrich	Cat# 73605
Dimethyloxalylglycine (DMOG)	Sigma Aldrich	Cat# 400091
Sodium pyruvate	Gibco	Cat# 11360070
Fixable viability dye eFluor™ 780	eBioscience	Cat# 65-0865-14
Cell Proliferation Dye-eFluor450	eBioscience	Cat# 65-0863-14
Mouse IL-2	PeproTech	Cat# 212-12
Mouse IL-7	PeproTech	Cat# 217-17
Mouse IL-15	PeproTech	Cat# 210-15
Cas9 nuclease	Integrated DNA Technologies, IDT	Cat# 1081060
OVAI peptide (SIINFEKL)	AnaSpec	Cat# AS-62572-5
Critical commercial assays		
MojoSort™ Mouse CD8 T cell Isolation Kit	Biolegend	Cat# 480035
P3 Primary Cell 4D-Nucleofector™ X Kit	Lonza	Cat# V4XP-3024
Deposited data		
[U-^{13}C]glucose tracing in naive vs. activated CD8$^+$ T cells	This paper	National Metabolomics Data Repository: ST002362
[U-^{13}C]glucose tracing in NT, AOA, or EGCG treated CD8$^+$ T cells	This paper	National Metabolomics Data Repository: ST002363
[U-^{13}C]glucose tracing in WT, GOT1$^{-/-}$ or GLUD1$^{-/-}$ CD8$^+$ T cells	This paper	National Metabolomics Data Repository: ST002364
[U-^{13}C]glutamine tracing in WT, GOT1$^{-/-}$ or GLUD1$^{-/-}$ CD8$^+$ T cells	This paper	National Metabolomics Data Repository: ST002365
Extracellular metabolome of blank [U-^{13}C]glucose tracing media or post activated CD8$^+$ T cell culture	This paper	National Metabolomics Data Repository: ST002372
Extracellular metabolome of blank media or post activated CD8$^+$ T cell culture	This paper	National Metabolomics Data Repository: ST002373
Metabolomics analysis of WT vs. GOT1$^{-/-}$ CD8$^+$ T cells	This paper	National Metabolomics Data Repository: ST002374
Metabolomics analysis of WT vs. GOT1$^{-/-}$ CD8$^+$ T cells with or without serine	This paper	National Metabolomics Data Repository: ST002375
Experimental models: Organisms/strains		

REAGENT or RESOURCE	SOURCE	IDENTIFIER
C57BL/6J	Jackson Laboratories	N/A
Cd4-Cre	Jackson Laboratories	N/A
CD90.1	Jackson Laboratories	N/A
CD45.1	Jackson Laboratories	N/A
OT-I TCR transgenic mice	Jackson Laboratories	N/A
P14 TCR transgenic mice	Dr. David A. Hildeman (Cincinnati Children's Medical Center)	N/A
Got1 floxed mice	MRC Harwell Institute	N/A
Glud1 floxed mice (University of Geneva)	Dr. Pierre Maechler	N/A
Oligonucleotides		
Ctrl gRNA: 5′-GCACUACCAGAGCUAACUCA-3′	Synthego	N/A
Vhl g1: 5′-AGGUCAUCUUUGGCUCUUCA-3′	Synthego	N/A
Vhl g2: 5′-UUUGGCUCUUCAGGGAUGCG-3′	Synthego	N/A
Vhl g3: 5′-AGGGAUGCGGGGACCCAUGA-3′	Synthego	N/A
Software and algorithms		
FlowJo	FlowJo	v.10.3
GraphPad Prism	GraphPad Prism	v.7 and 8
MultiQuant	AB Sciex	v2.1
Metaboanalyst	N/A	https://www.metaboanalyst.ca/
Other		
FACSCelesta	BD Biosciences	https://www.bdbiosciences.com/en-us/products/instruments/flow-cytometers/research-cell-analyzers/facscelesta
Applied Biosystems StepOnePlus™ 96-well Real-Time PCR System	Thermo Fisher Scientific	Cat# 4376600
XF96 Extracellular Flux Analyzer	Agilent	https://www.agilent.com/en/product/cell-analysis/real-time-cell-metabolic-analysis/xf-analyzers/seahorse-xfe96-analyzer-740879